The 8th European Congress on Computational Methods in Applied Sciences and Engineering
ECCOMAS Congress 2022
5-–9 June 2022, Oslo, Norway

HOMOGENIZATION OF THE CONSTITUTIVE PROPERTIES OF COMPOSITE BEAM CROSS-SECTIONS

MARTINA STAVOLE[1], RODRIGO T. SATO MARTÍN DE ALMAGRO[1], MARGUS LOHK[2] AND SIGRID LEYENDECKER[1]

[1] Institute of Applied Dynamics (LTD)
Friedrich-Alexander-Universität Erlangen-Nürnberg
Immerwahrstrasse 1, 91058 Erlangen, Germany
e-mails: martina.stavole@fau.de, rodrigo.t.sato@fau.de, sigrid.leyendecker@fau.de,
https://www.ltd.tf.fau.de

[2] Karl Storz Video Endoscopy Estonia (KSEE)
Pärnu mnt 556b, Laagri, 76401 Harju maakond, Estonia
email: margus.lohk@karlstorz.com, https://www.karlstorz.com/de/it/estonia-tallinn.htm

Key words: Composite materials, Homogenization, Effective constitutive properties, Cosserat rod

Abstract. When modelling slender bodies made of composite materials as beams, homogenized stiffness coefficients must be obtained. In [2, 3], analytic expressions for these are obtained by comparing the solutions of some Saint-Venant extension, bending and torsion 3D linear elasticity problems with their corresponding beam theory counterparts. In [2], the authors provide general expressions for the determination of these coefficients for multilayered beams.
The present work consists in the study of a homogenization procedure of the stiffness coefficients for circular cross-sections with two layers. This will help in the study of the constitutive behavior of unloaded shafts of endoscopes since their cross-section could be studied as a simplified model of a three-layers hollow circular cross-section. In preparation of this geometry, results of an experimental campaign carried out at KARL STORZ GmbH & Co. KG (Tallinn, Estonia) are presented in a second part of this paper. The purpose of the testing was the experimental characterization of the torsional stiffness of such devices.

1 INTRODUCTION

Flexible endoscopes are medical devices with a slender cylindrical geometry. These can be modelled using complex finite-element models and nonlinear 3D elasticity equations, but the computational cost of such an approach can be quite high. This is particularly true when considering their dynamics in confined environments, which is of great interest for practical application cases. Thus, we aim to develop a simplified mathematical formulation in terms of 1D beam-like objects. This can be a more efficient and effective approach to understanding their mechanical behaviour during operation. One of the critical points for the success of this simplification process is the characterization of their constitutive properties.

In general, the structure of an endoscope can be separated into an external part and an internal cavity where the instruments are housed. Our focus is on the outer part, denominated unloaded shaft, that is the most relevant in regards to its mechanical properties. It can be seen as a multi-layered hollow beam, namely as a composite structure composed of numerous layers of different materials. Fig. 1 shows the longitudinal and transversal sections of a shaft composed of four layers. Starting from the innermost one, in the composite cross-section there are a steel coil, a steel braided mesh, a plastic cover partially embedded in the mesh, and an outermost layer of plastic. It is important to remark that the coil is only attached to the overall structure at the ends of the shaft, and this means that it can move relative to the other layers. The latter are firmly connected to each other, such that no relative motion can take place.

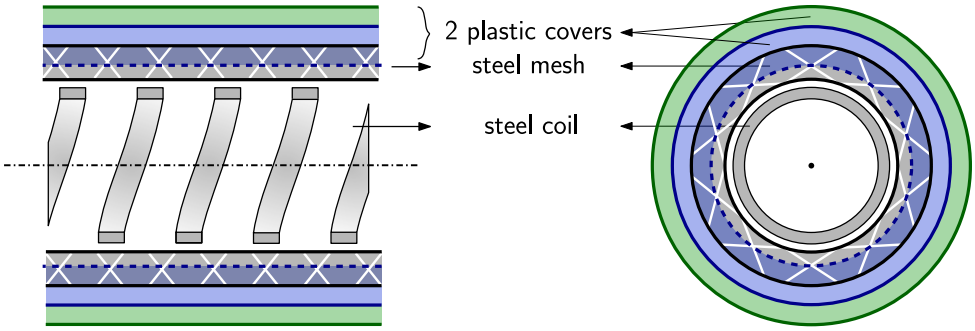

Figure 1: Longitudinal (left) and transversal (right) sections of an endoscope. In the picture, the overlap between the inner plastic cover (blue) and the steel mesh (grey with white crosses) is meant to convey the thermal embedding of the latter in the former.

Despite the idealized model, the mechanical behaviour is still hard to catch due to the nonlinearities involved in the problem. Moreover, when working with composite structures, there is one more difficulty: the homogenization of the different materials composing the cross-section, i.e. how to properly model multi-material structures from micro-scale to macro-scale. In this paper, an analytical determination of effective stiffness parameters presented in literature [1, 2] is taken into account, referring especially to the study case of a two-layers circular cross-section. This investigation represents the first step in the homogenization process of the constitutive properties of unloaded shafts. The theory can be indeed expanded to a three-layers cross-section, which is close to the shafts' geometry, as it will be later explained in Section 3. With necessary considerations, the expanded formulation will be correlated to an experimental campaign performed

on unloaded shafts for torsional stiffness characterization. For this purpose, the test results are shown in the second part of this work.

2 MATERIALLY COUPLED AND UNCOUPLED APPROACHES

2.1 Theoretical background

We want to obtain homogenized stiffness coefficients to characterize the mechanical behaviour of the beam. We consider two approaches to do so. One is a simple *materially uncoupled* approach, where each material is assumed to behave independently from the others. This leads to additive contributions to the stiffnesses. The other is a *materially coupled approach*, where the deformation of each material must be compatible with that of the rest, leading to a continuous deformation field across all cross-sections in the equivalent 3D elasticity problem.

This coupled approach is described in [1, 2], where the authors investigate the mechanical behaviour of composite elastic beams modelling them as 1D Cosserat continua (see [4, 3, 5] for details). The beams are modeled by deformable curves, characterized by a position vector, and a triad of directors attached to every point along the curve. The triad describes the orientation of the cross-sections, which are assumed to remain planar, during deformation.

In [2], circular two-layer piecewise homogeneous beams made of isotropic materials, as shown in Fig. 2, are studied. The cross-section is divided into a core and a face, characterized by different material and geometric parameters (namely, their respective density ρ, Young's modulus E, Poisson's ratio ν, radius of the inner circle R_1 and of the outer circle R_2) and welded together in such a way that no separation can occur during deformation.

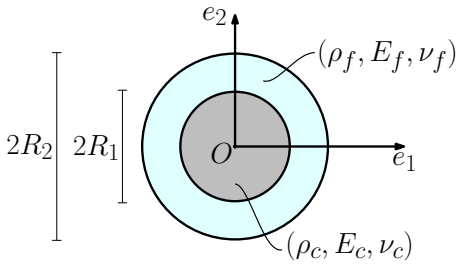

Figure 2: Mock-up of circular two-layer piecewise homogeneous sandwich cross-section with inner core (in grey) and outer face (in light blue)

They derive the constitutive equations for elastic composite rods in the infinitesimal deformation regime, with a linear elastic constitutive model and obtain the effective extensional, bending and torsion stiffness properties of thin rods. They do so by comparing the solutions of extension, bending and torsion problems of a beam with those obtained from the three-dimensional linear Saint-Venant problem. Similarly, they compare frequency analysis results for the 1D and 3D elasticity problems to estimate the shear stiffness.

This is a materially coupled approach to homogenization because in the solution of the Saint-Venant problem, compatibility conditions are imposed to the deformation of each material of the

section, which couples their behaviour. In the particular case described in Fig. 2, the effective homogenized stiffness properties are expressed as follows (see [2]):

$$C_1 = C_2 = \frac{\pi}{4}\left[E_c R_1^4 + E_f\left(R_2^4 - R_1^4\right)\right] - \frac{\pi\left(\nu_c - \nu_f\right)^2\left(R_2^4 - R_1^4\right)R_1^4}{2\left[\alpha_c R_1^4 + \beta_c R_2^4 + \alpha_f\left(R_2^4 - R_1^4\right)\right]} \tag{1}$$

$$A_3 = \pi\left[E_c R_1^2 + E_f\left(R_2^2 - R_1^2\right)\right] - \frac{4\pi\left(\nu_c - \nu_f\right)^2\left(R_2^2 - R_1^2\right)R_1^2}{\left(\alpha_c - \beta_c\right)R_1^2 + 2\beta_c R_2^2 + \left(\alpha_f - \beta_f\right)\left(R_2^2 - R_1^2\right)} \tag{2}$$

$$C_3 = \frac{\pi}{2}\left[G_c R_1^4 + G_f\left(R_2^4 - R_1^4\right)\right] \tag{3}$$

$$A_1 = A_2 = \kappa\pi\left[G_c R_1^2 + G_f\left(R_2^2 - R_1^2\right)\right]\frac{\rho_c R_1^4 + \rho_f\left(R_2^4 - R_1^4\right)}{R_2^2\left[\rho_c R_1^2 + \rho_f\left(R_2^2 - R_1^2\right)\right]} \tag{4}$$

with $\alpha_i = (3-4\nu_i)\beta_i$, $\beta_i = 1/(2G_i)$ and $G_i = E_i/(2(\nu_i)+1)$ (shear modulus) for the corresponding layers.

One can recognize two contributions to these parameters. On the one hand, we have the uncoupled contribution to the stiffness. On the other hand, we find an additional term stemming from the coupled formulation proposed by [1, 2]. For the bending stiffnesses C_1, C_2 and the axial stiffness A_3, the coupling terms are additive, while the coupling term is multiplicative for the shear stiffnesses A_1, A_2. No additional term is present in the torsional stiffness C_3. It should be noted that most of these coupling contributions vanish whenever the Poisson's ratios of contiguous components coincide.

The comparison between the two theories is useful to investigate the influence of coupling between layers. It will serve to inform us about the order of the corrections we should expect in the many-layer case found in unloaded shafts.

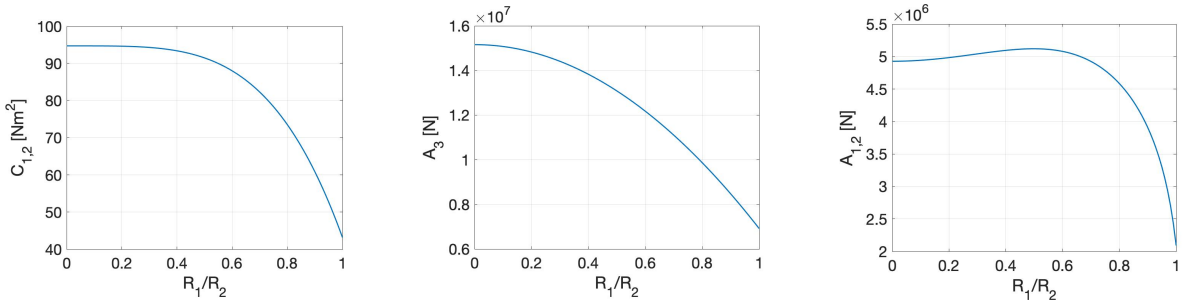

(a) bending stiffness (b) axial stiffness (c) shear stiffness

Figure 3: Materially coupled stiffnesses: properties of a cross-section made of steel face and polypropylene core

2.2 Numerical comparison

In this section, a cross-section composed by a steel face and a polypropylene core is taken into account for analyzing a comparison between additive and coupled theories. The mechanical parameters characteristic of each material are shown in Table 1. In Fig. 3, the homogenized coupled bending, axial and shear stiffness parameters are plotted versus the ratio between the inner and outer radii. It is clear that for a ratio close to one, the polypropylene area increases compared to the steel one, and consequently the stiffness properties decrease.

The comparison between the materially uncoupled and coupled approaches is expressed in terms of absolute and relative discrepancies. In (5) and (6), K is either a bending stiffness parameter C_1, C_2 from (1) or the axial stiffness A_3 from (2), for which the coupling terms are added. For the shear stiffnesses A_1, A_2 in (4) containing a multiplicative coupling contribution, a relative discrepancy (7) is computed, while no discrepancy can be computed for the torsional stiffness (as C_3 contains no coupling contribution, see (3)).

$$\Delta_{\text{abs}} K = K_{\text{coupled}} - K_{\text{uncoupled}} \tag{5}$$

$$\Delta_{\text{rel}} K = \left(\frac{K_{\text{coupled}} - K_{\text{uncoupled}}}{K_{\text{uncoupled}}} \right) 100 \tag{6}$$

$$\Delta_{\text{rel}} A_{1,2} = \left(\frac{A_{1,2\text{coupled}}}{A_{1,2\text{uncoupled}}} - 1 \right) 100 \tag{7}$$

Those contributions are shown in Fig. 4, Fig. 5 and Fig. 6 respectively for bending, axial and shear stiffness where for the latter only the relative difference was computed.

Table 1: Material properties of the two layers

	steel (face)	polypropylene (core)
E $[N/m^2]$	1.93E+11	1.30E+09
ν $[-]$	0.265	0.43

In general, one can see that the discrepancy between the materially uncoupled and coupled approaches increases when the inner radius R_1 approaches the outer radius R_2. However, from the relative discrepancies in Fig. 4b for bending and Fig. 5b for axial stiffness, one can see that the discrepancy in both cases is less than 0.1 % and 0.2 % respectively. However, in the case of shear stiffness, Fig. 6 shows a discrepancy of about 50%.

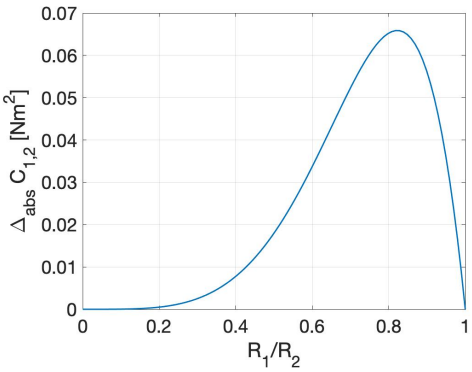

(a) absolute discrepancy

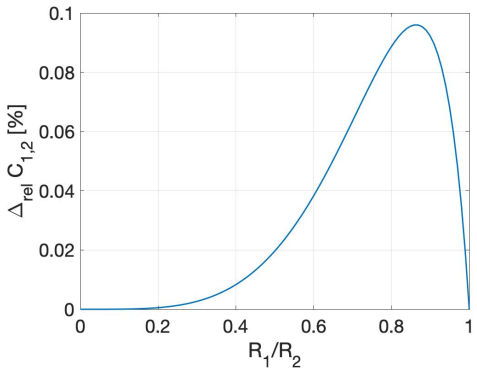

(b) relative discrepancy

Figure 4: Comparison of bending stiffness in materially coupled and uncoupled approaches

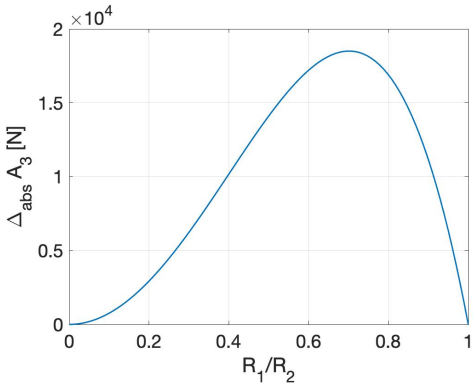

(a) absolute discrepancy

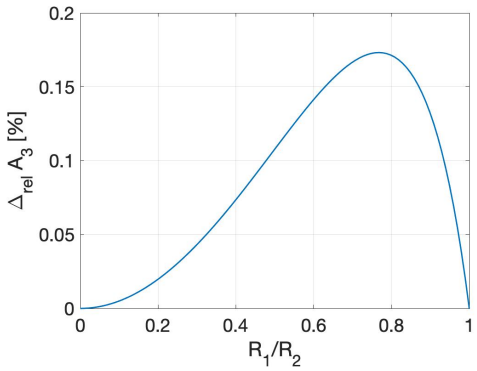

(b) relative discrepancy

Figure 5: Comparison of axial stiffness in materially coupled and uncoupled approaches

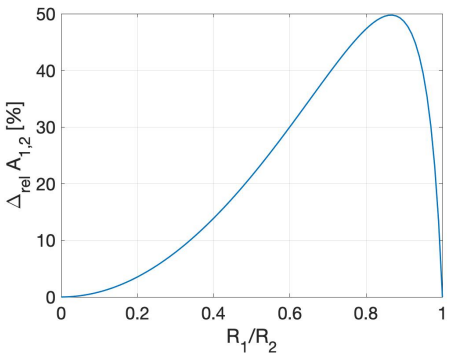

Figure 6: Comparison of shear stiffness in materially coupled and uncoupled approaches

3 PERSPECTIVES FOR MODEL IMPROVEMENT

Coming back to the endoscope depicted in Fig. 1, one can model it as four-layered cross-section with the hollow interior (considered as a layer), a steel mesh, and the two outermost layers of plastic. Given the considerations made earlier, the coil will not be considered coupled to the rest, and, assuming its contribution to shear is negligible, it can be added *a posteriori*.

Although possible to differentiate them, we will actually treat the two plastic layers as a single one. The reason lies in the industrial manufacturing process. Once heated up in the oven, the two plastic covers melt together and their material properties change both due to thermally-induced molecular rearrangement and newly formed cross-links between materials in a manner difficult to predict. In the future, we aim to model the unloaded shaft with three layers as indicated in Fig. 7.

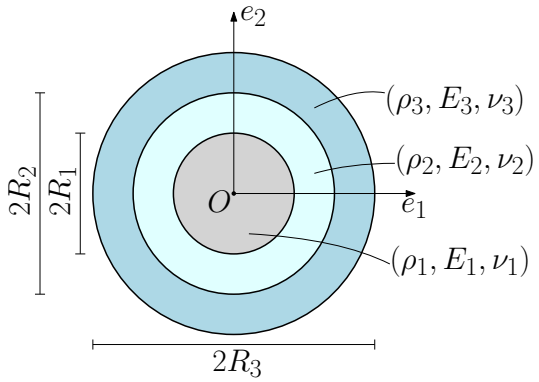

Figure 7: Three-layers piecewise homogeneous cross-section

The first step will be to derive the effective stiffness properties based on the materially uncoupled approach. The analytical expressions are a straight-forward extension of the uncoupled parts in (1)-(4). However, the respective material parameters (particularly Young's modulus and Poisson's ratio) of the outer layer are unknown. They will be fitted with the help of experimental data. It will be interesting to examine, how close a three-layer model can approximate the data and to what extent the known uncoupled data of the plastic covers applies.

The second step, which is by far more involved, will be to derive the analytical expressions of the materially coupled approach for the three-layers case. Again, the discrepancy between the materially uncoupled and coupled approach will be investigated, as well as the question, which approach can reach a more accurate prediction of the experimental data.

In preparation of these more complex models and their evaluation, we start by analyzing our first experimental results in the next section.

4 EXPERIMENTAL TESTING OF UNLOADED ENDOSCOPE SHAFTS

An experimental campaign has been carried out at Karl Storz Video Endoscopy Estonia (KSEE), for which they provided several samples of three different endoscope models. For each type, four to five samples have been tested. The internal structure of all types of shafts is as shown in Fig. 1, with small changes in the outer radius.

The torsion testing machine used for the experiments is shown in Fig. 8. The experimental setup is relatively standard. Both ends of the sample are clamped onto the machine. One of the clamps is mounted onto a rail that allows axial displacements of the clamp in order to accommodate different sample lengths and to eliminate compression or bending strains. The other clamp is equipped with an actuator (a servomotor) that applies angular displacements and sensors measuring the axial torque exerted by the sample in response. For our testing, the distance between the two clamping devices was set to 10 cm. To analyze the influence of the internal spring under torsion, the torsion tests have been performed in clockwise and anticlockwise directions. The sampling frequency was 16.67 Hz and the rotations took place three times in the clockwise and anticlockwise direction between the angles $\theta = -4$ and $\theta = 4$ for endoscope 1 and 3 and four times between $\theta = -5$ and $\theta = 5$ for endoscope 2.

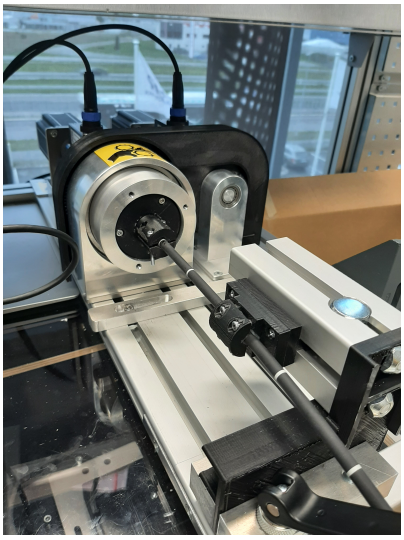

Figure 8: Torsion testing machine at Karl Storz Estonia

4.1 Analysis of the experimental results

The experimental data for the three endoscope types are shown in Fig. 9, 10 and Fig. 11, respectively. For positive torsion angles $\theta > 0$, the shaft has been rotated clockwise, and anticlockwise for $\theta < 0$. For each endoscope type, the same data is plotted in all respective subfigures, however together with different model fits. It is quite noticeable, that the results of the first and third type of endoscope are similarly scattered, while the data of the second type is closely concentrated around a line. This fact also becomes obvious when looking at the very

small confidence intervals of the fits for endoscope 2 in Tab. 2 and Tab. 3 which are described next.

In order to fit the parameters of a material model to the data, a least-squares regression analysis has been carried out. With this method, the model parameters are identified by minimizing the sum of squared deviations of the model-predicted torque $T(\theta)$ from the measured torque in the complete interval of torsion angles θ. Two different models have been taken into account, an affine model characterised two parameters, the slope C_3 and the offset T_o, and a linear model based on C_3 only, reading

$$\begin{aligned} T(\theta) &= C_3\theta + T_o \quad \text{(affine regression model)} \\ T(\theta) &= C_3\theta \quad \text{(linear regression model)} \end{aligned} \tag{8}$$

Note that for homogeneous circular cross-sections, the torsional stiffness $C_3 = GJ$ is given in terms of the shear modulus $G = E/(2(\nu+1))$ and the polar moment of the area J. However, for composite material, such a split in material and geometric parameters is not necessarily possible.

For the three types of endoscopes, Fig. 9, 10 and Fig. 11 show the data together with the affine fit in subfigure (a) and with the linear fit in subfigure (b), respectively. In the figures, θ is the twisting angle per unit length. The results are summarized in Table 2, where the mean values are the fitted parameters to define the model and also the confidence intervals are shown. It can be seen, that T_o takes very small values for all types of endoscopes. Further, for all endoscope types, the fitted torsional stiffness properties from the affine and the linear model are very similar. This means that the systematic error due to initial offsets had little impact. Moreover, the identified torsional stiffness properties do not differ much between the endoscope types. Indeed, the shafts are pretty similar in geometry and structure, there are only small differences in the outer diameters.

Table 2: Least-squares regression analysis on the three endoscope types

type number	model parameters	affine		linear	
-	-	mean	confidence	mean	confidence
endoscope 1	C_3 $[Nm^2]$	0.0594	5.11 e^{-5}	0.0593	5.19 e^{-5}
	T_o $[Nm]$	-5.76 e^{-3}	8.76 e^{-5}	-	-
endoscope 2	C_3 $[Nm^2]$	0.0573	1.23 e^{-21}	0.0573	1.23 e^{-21}
	T_o $[Nm]$	7.06 e^{-12}	2.37 e^{-21}	-	-
endoscope 3	C_3 $[Nm^2]$	0.0500	3.22 e^{-5}	0.0498	3.22 e^{-5}
	T_o $[Nm]$	-1.23 e^{-2}	5.69 e^{-5}	-	-

To investigate the influence of the internal coil on the torsional stiffness, the clockwise (winding of the coil) twists have been studied separately from the anticlockwise twists (unwinding of the coil). The data together with the separate linear fits for $\theta < 0$ and $\theta > 0$ are shown in subfigure (c) of Fig. 9, 10 and Fig. 11, respectively for the different endoscope types. The resulting parameters are summarized in Table 3. It can be noticed that there is no difference in the clockwise or anticlockwise identified torsional stiffness for endoscope 2, while there is a

small difference for endoscope 1 and a larger one for endoscope 3. Due to many uncertainties affecting the production process and the life-time of the shafts, it is very difficult to model their behaviour.

Table 3: Least-squares regression analysis on the three shaft models: clockwise and anticlockwise directions

type number	torsional stiffness	clockwise		anticlockwise	
-	-	mean	confidence	mean	confidence
endoscope 1	C_3 $[Nm^2/rad]$	0.0572	1.30 e^{-4}	0.0616	1.39 e^{-4}
endoscope 2	C_3 $[Nm^2/rad]$	0.0573	3.01 e^{-21}	0.0573	3.19 e^{-21}
endoscope 3	C_3 $[Nm^2/rad]$	0.0439	6.47 e^{-5}	0.0560	1.20 e^{-4}

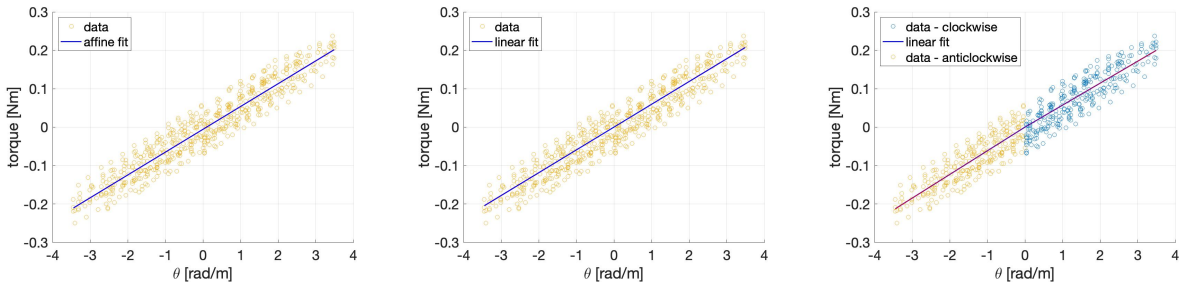

(a) affine fit (b) linear fit (c) clockwise and anticlockwise fit

Figure 9: Regression analyses: first endoscope model

5 CONCLUSIONS AND FUTURE WORK

The numerical comparison between the materially coupled and uncoupled approaches to model the effective stiffness of two-layer cylindrical beams illustrates that for the axial and bending stiffness parameters, the difference is negligible for small ratios of inner to outer radius. However, for the shear stiffness the discrepancy is quite high, reaching even 50 %.
The analysis of the experimental torsion test data revealed that a linear model can represent the data quite well with very small confidence intervals (of the order of 10^{-4}) for all experiments. However, the scattering of data points was noticeably smaller (10^{-21}) endoscope type 2. The presence of the coil causes a slightly stiffer but negligible behaviour in the anticlockwise (unwinding) case for the endoscope types 1 and 3.
As mentioned in Section 3, a three-layers model might be able to represent the behaviour of the unloaded endoscope shafts much better and shall be investigated in the future. Effective stiffness properties will be derived for the materially coupled and uncoupled approaches and the material parameters will be fitted with the help of experimental data. For this purpose, a more detailed experimental testing campaign has already been started, investigating bending

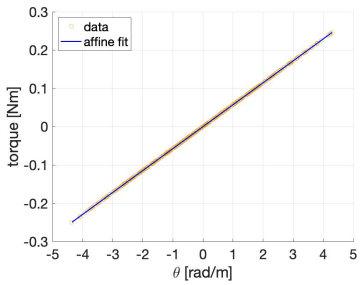

(a) affine fit

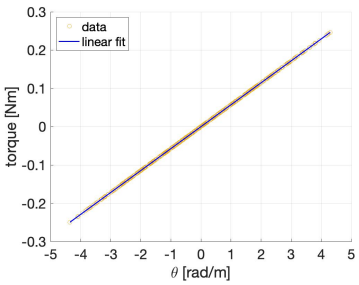

(b) linear fit

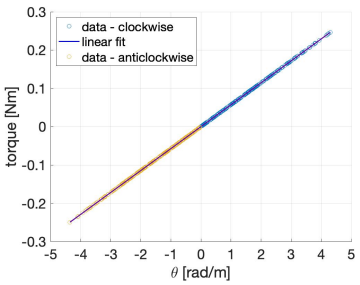

(c) clockwise and anticlockwise fit

Figure 10: Regression analyses: second endoscope model

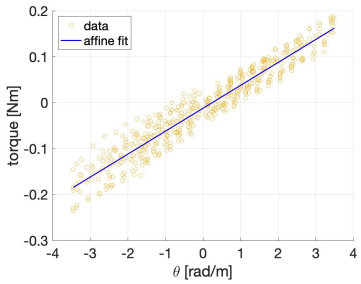

(a) affine fit

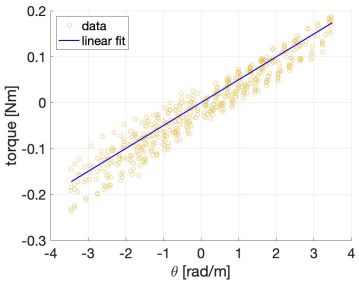

(b) linear fit

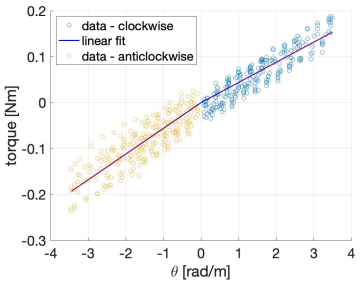

(c) clockwise and anticlockwise fit

Figure 11: Regression analyses: third endoscope model

and torsional deformation as well as the influence of several and separate layers.

Acknowledgements

This project has received funding from the European Union's Horizon 2020 research and innovation programme under the Marie Skłodowska-Curie grant agreement No 860124.

REFERENCES

[1] N. I. Muskhelishvili. Some basic problems of the mathematical theory of elasticity. Noordhoff, Groningen. (1963) *17404(6.2)*: 1,

[2] M. Bîrsan, D. Pietras and T. Sadowski. Determination of effective stiffness properties of multilayered composite beams. Springer, *Continuum Mechanics and Thermodynamics* (2021), 1–23.

[3] M. Bîrsan, H. Altenbach, T. Sadowski et al.. Deformation analysis of functionally graded beams by the direct approach. *Composites Part B: Engineering* (2012), Vol. **43(3)**:1315–1328.

[4] H. Altenbach, M. Bîrsan and V. Eremeyev. Cosserat-type rods. Springer, *Generalized Continua from the Theory to Engineering Applications* (2013), 179-–248.

[5] S. Leyendecker, J. E. Marsden and M. Ortiz. Variational integrators for constrained dynamical systems. *ZAMM - Zeitschrift für angewandte Mathematik und Mechanik* (2008), Vol. *88*: 677-708.